Visual comfort assessment of smart photovoltachromic windows

ARTICLE *in* ENERGY AND BUILDINGS · OCTOBER 2013

Impact Factor: 2.88 · DOI: 10.1016/j.enbuild.2013.06.019

4 AUTHORS, INCLUDING:

Francesco Fiorito
University of New South Wales
30 PUBLICATIONS **64** CITATIONS
SEE PROFILE

Alessandro Cannavale
Università del Salento
17 PUBLICATIONS **217** CITATIONS
SEE PROFILE

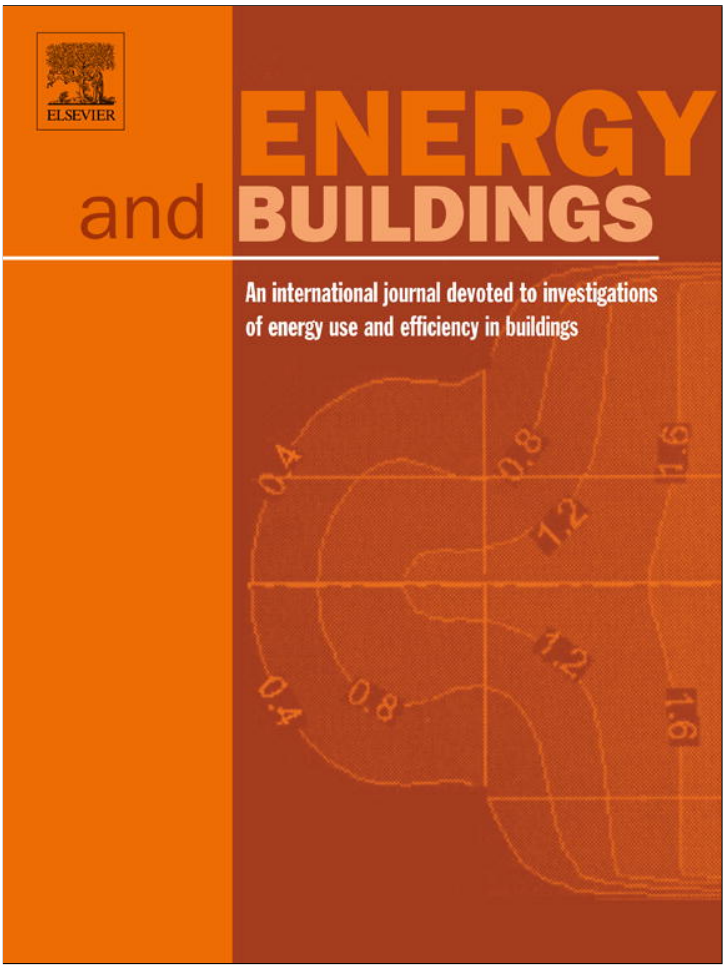

Energy and Buildings 65 (2013) 137–145

Contents lists available at SciVerse ScienceDirect

Energy and Buildings

journal homepage: www.elsevier.com/locate/enbuild

Visual comfort assessment of smart photovoltachromic windows

Alessandro Cannavale[a,1], Francesco Fiorito[b,*,1], Debora Resta[c], Giuseppe Gigli[a,d,e]

[a] Center for Biomolecular Nanotechnologies@UniLe, Istituto Italiano di Tecnologia, via Barsanti, 73010 Arnesano, (Le), Italy
[b] The University of Sydney, Faculty of Architecture, Design & Planning, 148 City Road, 2006 Sydney, Australia
[c] Independent Engineering Professional, Italy
[d] NNL – National Nanotechnology Laboratory, CNR Istituto Nanoscienze, Distretto Tecnologico, Via Arnesano 16, 73100 Lecce, Italy
[e] Dipartimento di Matematica e Fisica "E. De Giorgi", Universita' del Salento, Via per Arnesano, 73100 Lecce, Italy

ARTICLE INFO

Article history:
Received 30 January 2013
Received in revised form 7 May 2013
Accepted 9 June 2013

Keywords:
Photovoltachromic
Building integration
Photoelectrochromic
Visual comfort
Solar control
Transparent building envelope

ABSTRACT

An experimental study of photovoltachromic (PVCC) devices for dynamic solar control in buildings is presented. The fabricated devices underwent a complete opto-eletctrical characterization and the results obtained were employed as an input for the simulation of building integrated multifunctional windows. This multidisciplinary activity aims at achieving relevant feedbacks from the simulation of real large area devices in order to adjust and even direct further experimental efforts, before reaching the production phase. Devices having different electrochromic capacitances were used and the optical measurements became useful inputs for the simulation task. Simulation's results turned into feedbacks concerning the modulation of the transmittance spectra, the colour of bleached devices, the scale-up of PVCCs. Devices used in the current work showed a power peak of 4.22 mW/cm^2 at the maximum power point and a smart modulation of optical transmittance of 50.16% (at 700 nm). Simulations of natural light penetration in office buildings showed that the integration of PVCCs in traditional windows could dramatically increase indoor visual comfort. An increase of the average UDI for a typical room up to 71.8% and a decrease of intolerable glare levels (DGP higher than 0.45) down to 12% were the major benefits of the substitution of traditional clear glasses with integrated PVCCs.

1. Introduction

1.1. Smart electrochromic windows: integration strategies and comfort issues

In recent years several research activities have been directed towards smart materials and devices, in order to achieve a dynamic solar control in transparent building envelopes (often referred to as "smart windows" or "switchable glazing") [1,2]. A large number of studies are currently in progress about electrochromic windows [3]. Such devices astonishingly enhance the energy performances of windows with respect to conventional shading and solar control devices, with several other fallouts: reduction of cooling, heating and ventilation loads, and a considerable reduction of artificial lighting due to a correct use of daylighting as a source of illumination [4]. An interesting paper by Azens et al. [5] has investigated the energy savings obtained by using electrochromic glazing eventually showing how smart windows are able to yield energy efficiency as well as comfort for the users of the building, using daylighting as an efficient source of illumination, even outperforming photovoltaic façades in terms of energy savings.

However in many applications of smart windows an efficient strategy for solar control contrasts with the requirement of a visual perception of external environment, due a substantial reduction of the visual transmittance of Electrochromic (EC) windows.

The main issue of building integration of EC devices, which still remains open, is the necessity of the adoption of advanced control strategies, in order to automatically balance thermal and visual comfort parameters according to the fluctuation of incident solar irradiance. Detailed assessment of control strategies of EC windows operational parameters [6–9] showed how switching settings could dramatically change indoor comfort levels and energy consumptions. As a matter of fact, energy consumption variations related to different control strategies based on indoor lighting levels, time-schedule control, or more complex fuzzy logics, have considerable deviations (24% for winter heating, 39% for summer cooling, 20% for winter electricity and even 63% for summer electricity), always with the same boundary conditions [7]. Furthermore, local thermal discomfort is also noticeable in EC windows, as the portion of solar radiation not used for daylight purposes is absorbed and re-irradiated by the glass.

* Corresponding author. Tel.: +61 2 9351 5601; fax: +61 2 9351 3031.
E-mail addresses: francesco.fiorito@sydney.edu.au, f.fiorito78@gmail.com (F. Fiorito).
[1] These authors contributed equally to the work.

0378-7788/$ – see front matter © 2013 Elsevier B.V. All rights reserved.
http://dx.doi.org/10.1016/j.enbuild.2013.06.019

1.2. Photoelectrochromics and photovoltachromics: novel promising devices for building integration

A very promising category of "smart" chromogenic devices is, instead, represented by photoelectrochromics (PECs), a special kind of self-powered smart windows [10]. They are electrochemical cells consisting of two electrodes, separated by a redox electrolyte. The photoanode is coated by a layer of dye-sensitized mesoporous titanium dioxide (on a transparent conductor), whereas the counter electrode shows a cathodic electrochromic material (generally WO_3). Several architectures have been proposed for these devices, especially because the colouration process is self-generated and does not require any external voltage, being activated depending on the available irradiance.

Some years later Georg et al. [11] proposed an alternative cell's architecture, with a similar working principle. Other device architectures have been explored in the last decade [12,13] and several polymeric materials have been used as electrochromic layers as well as poly(3,4-ethylenedioxythiophene) (PEDOT) and polyaniline (PANI) [14]. Starting from these remarks, the natural technological evolution of this class of devices should be represented by an integrated photovoltaic powered (PV–EC) window, also considering that the operational characteristics of both PV and EC technologies are highly compatible. A small area of PV cells could in fact provide sufficient electric power to operate a large-area EC window. In spite of these considerations, during the last ten years, just a couple of design options have been explored in this contest.

In 2009, for the first time, Wu et al. [15] reported a novel device, namely a photovoltachromic cell (PVCC), composed of a patterned WO_3/Platinum electrochromic electrode and dye-sensitized TiO_2 NP photoanode, first demonstration of a reliable approach to conveniently integrate PV and PEC technologies. Energy conversion efficiency exhibited by this first PVCC was about 0.5% and it was not possible to manage PV and PEC functionalities separately. The charge transfer between platinum and the electrolyte gives PVCCs photovoltaic characteristics. The platinum catalyser also enhances the colouration kinetics reducing colouring/bleaching times, with respect to the architectures of photoelectrochromic devices previously disclosed in literature [11,16].

More recently, we demonstrated [17] that an efficient tailoring in the electrolyte formulation can dramatically improve the electro-optical features of PVCCs, eventually achieving a good compromise between the photovoltaic performances and an adaptive modulation of optical absorption. Furthermore, a complete separation of two areas on the counterelectrode, one devoted to colouration (WO_3) and one to photovoltaic conversion (Pt) also allowed a bifunctional and interactive management of the device features. A photovoltaic conversion efficiency of 4.67% (at 700 W/m^2 of solar irradiance) and a transmittance modulation of 50.16% (at 700 nm) were obtained using a low-iodine electrolyte containing typical additives used in dye sensitized photo-electrochemical cells.

The abovementioned problems, related to the difficulties in PVs' building integration and to the automatic control strategies required for EC windows, are thus definitively solvable combining PVCCs with transparent building components: the automatic transparency modulation related to solar irradiance is a key characteristic. Nevertheless, visual properties of PVCCs strictly depend on design variables, such as thickness and materials adopted for the counter electrode, as demonstrated in previous works [17].

Photovoltachromic cells do not show significant limitations due to scale up processes and photoelectrodes, as in dye sensitized cells, will be soon produced by industries for large area modules worldwide [18], since a huge research effort has been produced in the latest years.

Therefore, the aim of the research activities here summarized was to drive the design process of PVCCs with the results of indoor visual comfort assessment, in order to choose the most suitable configuration. The method here proposed represents an iterative process of optimization and technology improvement, with the results of experimental activity taken as input for the simulation one and vice versa.

2. Methods

According to recent developments in the field of facade engineering design, building elements and components are implemented following the two alternative principles of "design driven research" or "research driven design" [19]. We decided to adopt the first one and to combine the experimental activities of production and characterization of smart photovoltachromic cells with simulations of natural light penetration in a standard test room with transparent surfaces equipped with these innovative devices.

The two distinct levels of activity – experimental and simulation one – are characterized by different parameters mutually influencing each other. The output of the experimental activity of design/fabrication/characterization of PVCCs turns into an input for the simulation tests described, giving important feedbacks for a re-design activity, which can take into account comfort parameters, not predictable in the laboratory activity. Then the feedback obtained through the modelling is used in order to drive the further design and fabrication of improved PVCC cells, in a cyclic process.

As already stated, photovoltachromic devices represent a novel class of multifunctional nanodevices, combining PV and PEC principles. Only a few bibliographic references have appeared so far [20–23], and they all concern small-area devices; no scale-up or development activities have already been demonstrated. Mainly for this reason, a preliminary study driven by computer modelling and concerning the effect of such a complex multifunctional device on the parameters of visual comfort can be a relevant spur to improve the design at the early stage of technology development. A similar approach has been used for predicting the efficacy of building integration strategies of small-area devices not already scaled up [24].

The key parameter chosen for driving the design of the new devices is the visual comfort assessment of indoor spaces. A test room, fully described in the experimental section and equipped with integrated PVCC windows has been modelled using DAYSIM [25].

DAYSIM is a validated Radiance-based programme, able to predict indoor annual luminance and illuminance levels under real-sky conditions derived from statistical weather files [26]. The programme combines a backward-ray-tracing algorithm with the daylight coefficient approach [27].

In the DAYSIM model all the opaque materials have been simulated using the RADIANCE *plastic* function, while the transparent materials (both PVCC and clear glass) have been simulated through the *glass* algorithm. More in detail, in RADIANCE based calculations *glass* simulates a special dielectric which accounts for the angular dependence of visual and solar transmission. The general algorithm takes into account the material's refraction – usually set at 1.52 – the incidence angle of solar radiation and the inter-reflections between the two surfaces of the panel [28]. The only input variable is the transmissivity (t_n, i.e. the amount of light that is not absorbed by the glass), which is related to the visual trasmittance T_n by means of the Eq. (1) [29].

$$t_n = \frac{\left(\sqrt{0.8402528435 + 0.007252239 \cdot T_n^2}\right) - 0.9166530661}{0.0036261119 \cdot T_n} \quad (1)$$

As DAYSIM does not manage automatically the variation of visual transmittance depending on incident solar radiation, a specific procedure has been designed in order to simulate the visual

comfort levels deriving from the adoption of PVCC devices in transparent envelopes.

After having identified an hourly simulation time-step, through DAYSIM the hourly solar irradiance on the façade's plane has been calculated as well as the respective window's visual transmittance. Then, integrating all the time-step over the statistical year, the selected visual comfort parameters have been calculated from the results of illuminance and glare simulations performed with DAYSIM.

Two are the comfort parameters chosen for assessing PVCC efficacy as a transparent material for windows: UDI and DGP.

Useful Daylight Illuminance (UDI) parameter, developed by Nabil et al. [30,31], is designed in order to interpret analyses of absolute daylight illuminance levels calculated on hourly-based meteorological data collected over a period of a full year. Useful Daylight Illuminances are defined as those falling within a range of values considered comfortable by the users. For the general aim of the current project a range of 100–2000 lux has been defined, according to previous literature reviews on occupants' preferences and behaviours [30]. Consequently, for each point of the desk plane, UDI is defined as the percentage of time in which the daylight illuminances fall within the selected range.

Daylight Glare Probability (DGP) developed by Wienold et al. [31] is a glare parameter which, contrarily to the other glare metrics, is able to predict the discomfort due to excess glare, taking into account not only the luminance gradient within the visual field but also the total vertical eye illuminance for a viewing hemisphere of 2π sr. Therefore, using this new metric, it is possible to consider as a glare source also the direct sunlight falling on a workplane. In the current work for the calculation of DGP we used the Eq. (2), which is already described in the most recent literature in the field [32]:

$$\mathrm{DGP} = 5.87 \times 10^{-5} \times E_v + 9.18 \times 10^{-5} \times \log_{10}^2 \left(1 + \Sigma_{i=1}^{2} \frac{L_{si}^2\, \omega_{si}}{E_v^{1.87}\, p_i^2}\right) \quad (2)$$

where E_v is the total vertical eye illuminance, while L_s, ω_s and P are respectively the luminance, solid angle and weight factor for each of the n glare sources i. According to [32] a DGP below 30% is considered imperceptible as less than 30% of the occupants perceive visual discomfort due to glare, while a DGP between 30% and 35% is considered perceptible. Furthermore DGP values greater than 35% are considered as disturbing or intolerable if higher than 45%. In the current work the DGP has been used as principal metric for assessing visual discomfort due to excessive glare and the values have been automatically calculated using the algorithm integrated in DAYSIM, as described in [32].

3. Experimental

3.1. Fabrication and electro-optical characterization of PVCC test cells

The preparation of photoelectrodes and counterelectrodes for the fabrication of devices employed in this research activity was diffusely described in [17]. The solar cells were assembled by facing the specifically patterned Pt/WO_3 counterelectrode onto the C-shaped dye sensitized photoelectrode. The two electrodes were assembled into a sandwich type cell and sealed with a Surlyn hot-melt gasket 50 mm thick. The redox electrolyte was introduced into the space of inter-electrodes through the hole pre-drilled on the back of the counter electrode. The holes were sealed up using Surlyn hot melt film and a cover glass. Optical transmittance spectra were observed by a VARIAN 5000 spectrophotometer. Photocurrent–voltage (I–V) and chrono-amperometric measurements were performed using a Keithley unit

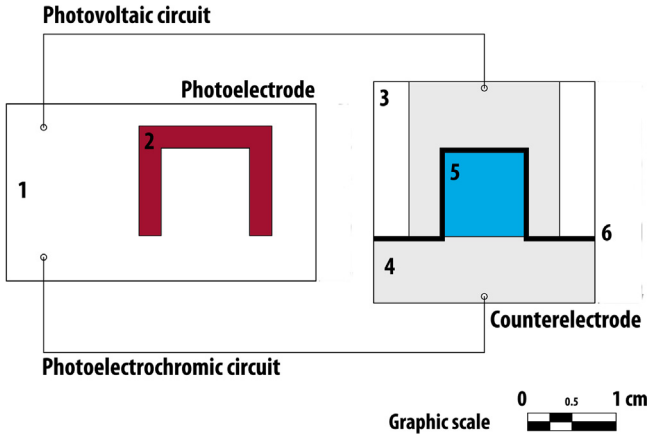

Fig. 1. Scheme of the device. (1) TCO, (2) dye sensitized titanium dioxide photoelectrode, (3) TCO, (4) platinum catalyzer, (5) tungsten oxide, (6) separation of circuits (by diamond-scriber).

(Model 2400 Source Metre). A Newport AM 1.5 Solar Simulator (Model 91160A equipped with a 300 W Xenon Arc Lamp) served as a light source, and its light intensity (or radiant power) was calibrated to 100 mW/cm^2 using a reference Si solar cell. A scheme and a cross-section of the devices are provided in Fig. 1, while a picture of the tested device in bleached and coloured state is shown in Fig. 2.

3.2. Test room settings and simulation parameters

The modelled test room has an indoor area of 20 m^2 (the plan in a 4 m × 5 m rectangle), with a net height of 3 m. The reason for the choice of such this space is to model a typical room within an office building. The room has two openings on the smaller sides: a door for the connection with the corridor (which is supposed not to give any contribution to natural light penetration) and a strip window of 6 m^2 area (equivalent to 20% of floor area and to 50% of south wall area).

The reference grid is composed of 336 surveying points (each point covering a 0.2 m × 0.2 m area) and has been set up at 75 cm above the floor level, corresponding to the ideal height of a work plane, according to the most affordable daylight monitoring protocols [33]. For avoiding edge effects due to the proximity of indoor and outdoor walls, the reference grid has been spaced out of 50 cm from each border. The view point is placed in the middle of the room at a distance of 2 m from the window and at a height of 1.1 m above the floor level, thus representing the position of a typical user seated. In order to maximize the glare phenomenon, the view point has been oriented towards the corner with the highest luminance gradient. As requested by the procedure for the calculation of DGP a view angle of 180° has been considered (corresponding to a fisheye camera).

The analysis has been carried out choosing as reference site the city of Bari, Italy (latitude 41°7′33″ N, longitude 16°52′6″ E and turbidity factor of 3), for its typical Mediterranean climatic conditions, such as levels of solar irradiance and outdoor temperature, and statistical weather files have been used as input for all the simulations [34].

Hence all the available data obtained as output from the simulation process depend on weather and orientation. For this reason, in order to consider properly the differences in visual comfort condition due to different exposures, two window's orientations have been tested: south and east.

All the analyses have been carried out for an entire year (derived from the weather file as statistical significant), selecting the working hours. In detail, two time slots have been selected: the morning

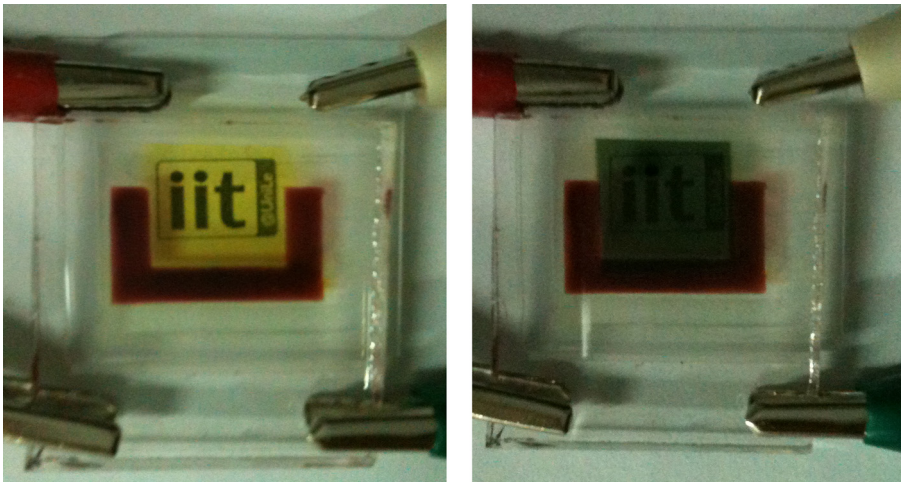

Fig. 2. Picture of the device in bleached and coloured conditions.

Table 1
Material properties for opaque elements.

Material	Colour	Reflectance [%]	Transmittance [%]	Specularity [%]	Roughness [%]
Indoor flooring	Stone grey	45.54	0.00	0.70	1.00
Internal walls	Beige 2k208	65.90	0.00	0.00	0.00
Indoor ceiling	White	85.77	0.00	0.00	0.00
Clear glass	Neutral	–	89.20	–	–

one between 8.00 am and 12.00 and the afternoon one between 1 pm and 5 pm for the weekdays (Monday to Friday).

As the general aim of indoor natural illuminance levels calculations was to compare PVCC windows with traditional clear ones, standard material properties included in Table 1 have been adopted for the intrados of building fabric (indoor flooring, internal walls, indoor ceiling and transparent surfaces).

In the following Table 2, the key parameters used in the radiance-based simulations are summarized. The ambient bounces parameter has been set at 5, in order to increase the precision of illuminance calculations and to take into account also multiple reflections on indoor surfaces [35]. The *ambient accuracy* and *ambient resolution* parameters have been set respectively at 0.1 and 300, in order to obtain, with a maximum scene dimension of 30 m, a minimum spatial resolution of 1 cm.

4. Results and discussion

4.1. Optical measurements

For two devices with a 230 nm and 300 nm thick tungsten oxide layer on ITO-coated glass, respectively named test cell A and test cell B, the transmission spectra were measured in the bleached condition (open circuit) and after a complete colouration process at different irradiation conditions (0.4 sun, 0.7 sun and 1 sun, where 1 sun is the standard solar radiation condition, equivalent to 1000 W/m^2). The results of measurements are summarized in Fig. 3. The test cell A did not show significant performances in optical modulation, as visible in Fig. 3a. The highest modulation of optical transmittance was instead obtained for test cell B. For this device, the peak values of transmittance obtained were 71% at 596 nm (bleached state) and 29% at 500 nm in the coloured state at 1000 W/m^2; the largest optical modulation was obtained for red light, at 657 nm. An optical modulation of 40% in the visible range was obtained. The transmittance attenuation was even higher in the infrared region (especially between 800 and 1250 nm). It must be highlighted that in the bleached state, the absorption of ITO strongly affects the spectrum. In the coloured state at 1 sun, the transmission is 30% with respect to the bleached state throughout the range 250–2500 nm. No linear dependence between optical modulation and irradiance was observed. In fact, the spectra corresponding to 700 W/m^2 and 1000 W/m^2 were almost coinciding. The thickest WO_3 layer (300 nm) exhibited the widest transmittance modulation as a consequence of its greatest volume of pathways available for the insertion of lithium cations. This characteristic dependence of ΔT on the film thickness has been previously demonstrated to be consistent with the variation of the optical density of the electrochromic layers [36].

4.2. Preliminary assessment of visual transmittance variability range

From the spectral distribution of transmitted (and thus of absorbed and reflected) radiation through each of the two test cells, the main solar and visual parameters have been calculated. Solar transmittance (T_{sol}), reflectance (R_{sol}) and absorbance (α_{sol}), as well as visual transmittance (T_{vis}), reflectance (R_{vis}) and absorbance (α_{vis}) are summarized in the following Table 3. While test cell A shows a limited modulation of solar and visual transmittance with respectively a gradient of 0.127 and 0.122, test cell B shows

Table 2
Set of parameters used for all radiance-based simulations.

Ambient bounces	Ambient division	Ambient super-sample	Ambient resolution	Ambient accuracy	Specular threshold	Direct sampling	Direct relays
5	1000	20	300	0.10	0.15	0.20	2

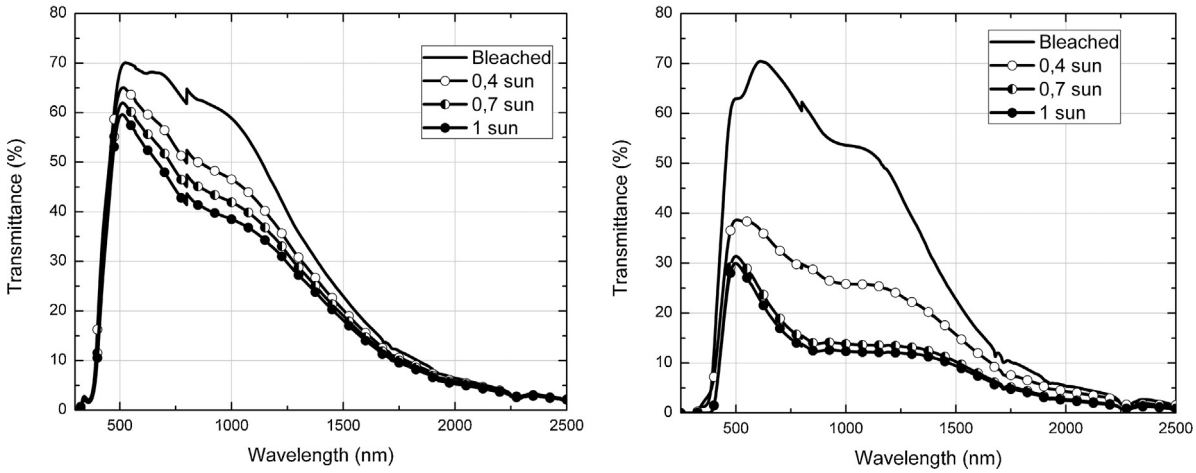

Fig. 3. Transmittance spectra at different irradiation conditions: (a) test cell A: 230 nm thick layer of tungsten oxide and (b) test cell B: 300 nm thick layer of tungsten oxide.

Table 3
Solar and visual characterization of test cell A and B.

	Solar parameters	T_{SOL}		R_{SOL}		α_{SOL}		T_{VIS}		R_{VIS}		α_{VIS}	
	Test cell	A	B	A	B	A	B	A	B	A	B	A	B
Solar radiation	BLEACHED	0.513	0.499	0.074	0.074	0.413	0.427	0.685	0.658	0.080	0.080	0.235	0.262
	0.4 SUN	0.448	0.267	0.074	0.074	0.478	0.659	0.625	0.377	0.080	0.080	0.295	0.543
	0.7 SUN	0.412	0.169	0.074	0.074	0.514	0.757	0.590	0.281	0.080	0.080	0.330	0.639
	1 SUN	0.386	0.156	0.074	0.074	0.540	0.770	0.563	0.263	0.080	0.080	0.357	0.657

Table 4
Correlation factor *r* between the populations of solar irradiances calculated for different steps of solar irradiance.

	10 W/m^2	50 W/m^2	100 W/m^2	200 W/m^2
A south	0.9998	0.9965	0.9878	0.9583
B south	0.9998	0.9959	0.9866	0.9560
A east	0.9997	0.9937	0.9780	0.9453
B east	0.9997	0.9922	0.9740	0.9393

a very good variation of both solar and visual transmittances, with gradients respectively of 0.343 and 0.395. For test cell B, the minimum visual transmittance (corresponding to a solar irradiance of 1000 W/m^2) is among the best achievable values to be adopted without compromising acceptance by users [37].

In order to reduce the computational time in DAYSIM, the values of simulated visual transmittances have been calculated for defined solar irradiance steps. A preliminary error analysis has been carried out in order to define the most suitable step's amplitude. Amplitudes of 10 W/m^2, 50 W/m^2, 100 W/m^2 and 200 W/m^2 have been considered and the corresponding values of visual trasmittances for both the two test cells have been compared with the ones calculated with the reference amplitude of 1 W/m^2.

In the following Table 4 the correlation factors "*r*" between the populations of values are summarized. For both east and south exposures a step's amplitude of 50 W/m^2 is the one that combines a good correlation factor – higher than 0.99 – with reduced calculation times and thus is the one selected for further simulations.

4.3. Visual comfort performances in test rooms

According to the statistical weather measurements for the city of Bari [34], the maximum solar irradiance on an unshaded south exposed vertical facade varies between 400 W/m^2 and 450 W/m^2 during the typical summer week (20–26 July) and between 200 W/m^2 and 550 W/m^2 during the typical winter week (10–16 February). Both for the test cell A and B the colouration process starts at about 5.00 am in summer and at about 7.30 am in winter. The minimum visual transmittance obtained is about 0.35 and 0.6 at 12.00 respectively for test cell B and A, while discolouration ends between 5.00 pm and 7 pm in winter and summer. For these reasons the visual transmittance changing of both the two cells completely intercepts the occupancy time of office spaces.

On east exposure, for both the test cell A and B, the colouration starts at about 4.30 am in summer and at about 7.00 am in winter. Although the bleaching process ends at the sunset, as for south-oriented facades, the colouration benefits end at about 12.00 noon. Therefore during all the seasons, the time in which the device is active intercepts a significant number of working hours.

The visual comfort analyses carried out show significant improvements of both the two selected parameters (UDI and DGP).

In detail Fig. 4 shows the distribution of UDI in the test room with an unshaded south-exposed window equipped with clear glass, PVCC A and PVCC B.

The adoption of a clear glass produces light levels inside the test room that are highly beyond the maximum tolerable by users. As a matter of fact, over the 336 sensor points, the minimum value of UDI registered is 5.8% (in proximity of the window), while the maximum registered value is 53.5% (in proximity of the partition between the test room and the corridor). Over the 336 sensor points the average UDI value is 26.1% and only the 7% of the sensor points exceed the 50% of UDI.

With the adoption of a window with the PVCC test cell A integrated, the minimum UDI increases to 8.6%, the maximum value to 85.4% and the average value to 44.4%. In this case more than the 43% of sensor points achieve a UDI higher than 50% over the entire year.

With the adoption of a window with the PVCC test cell B integrated, the increase in visual comfort due to natural light penetration is even more evident. Actually, over the entire test room, the minimum UDI increases up to 11.2%, the maximum UDI reaches the value of 96.9%, with an average UDI is 65.4%. With the adoption

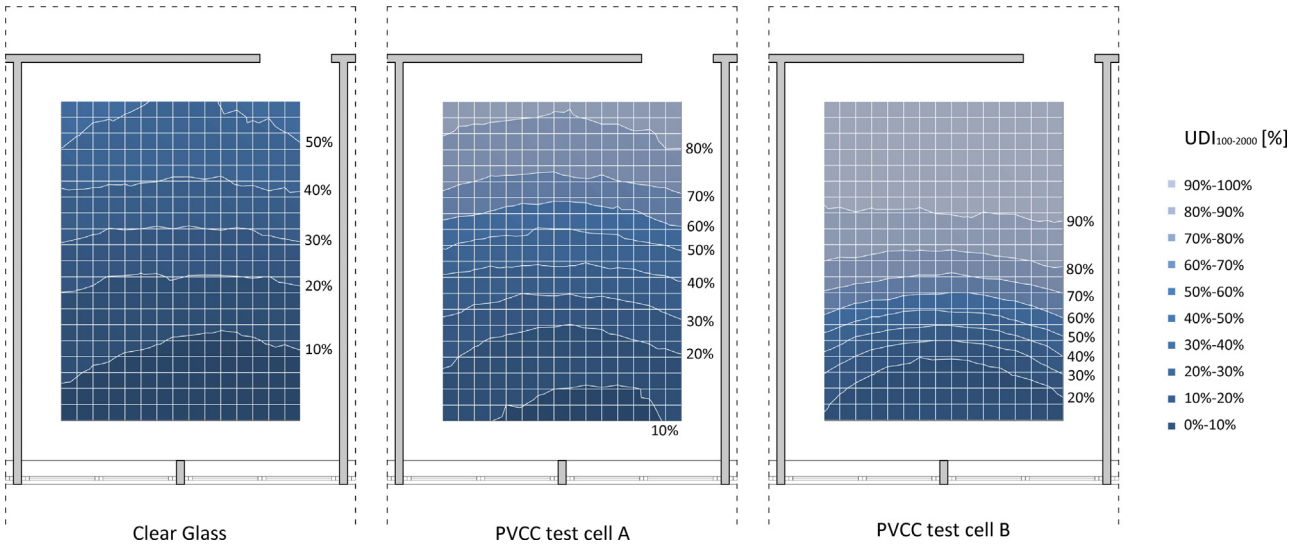

Fig. 4. Test room on south exposure: UDI during office hours (8.00–17.00).

of a window with a photovoltachromic cell B integrated into the transparent system, more than 68% of the room shows a UDI higher than 50%.

Fig. 5 shows the comparison of UDI parameter, considering a comfort range between 100 lux and 2000 lux, for the test room with the window oriented to east. The adoption of a window with clear glass produces light levels inside the test room that general exceed the upper comfort threshold (2000 lux). Therefore the minimum UDI value registered is 12.1%, the maximum one is 76.5% and less than half of the room (46% of sensor points) has UDI higher than 50%. Even with this orientation, the benefits in the adoption of a photovoltachromic glass instead of a clear one are evident. The integration of test cell A in transparent window panels allows increasing the minimum UDI to 22.6% and the maximum one to 88.5%, with an average value for all the sensor points of 60.5%. Furthermore more than 68% of the sensor points register a UDI higher than 50%.

The window showing higher performances, also with an east orientation, is the one equipped with photovoltachromic test cell B: only the 20% of the sensor points registered an UDI lower than 50%, with a minimum value of 28.9%, while more than 60% of the sensor point registered very high UDI (higher than 75%), with a maximum UDI registered of 93.2%. Therefore the average UDI value over the 336 sensor points is higher than 71%.

The excessive light exposure of indoor spaces equipped with unshaded windows also affects the glare probability. Actually, due to the presence of an unshaded non-tinted window exposed to south, an user seated in a typical office position perceives intolerable glare (DGP > 45%) for more than the 66% of working time, while only during the 16% of time the glare effect is imperceptible (DGP < 30%) or perceptible but not disturbing (35% < DPG < 45%). Fig. 6 summarizes the DGP values, grouped in hourly intervals for the test room with a south-oriented window. It is noticeable how the adoption of a photovoltachromic integrated glass produces a dramatic decrease of glare discomfort. The percentage of hours in which the glare is intolerable is reduced to 40% and to only 12% with the adoption of respectively the test cell A and the test cell B. This is mainly due to a reduction of the glare probability during the central hours of the working day (10–12 and 13–15).

Fig. 7 summarizes the DGP values, grouped in hourly intervals for the test room with an east-oriented window. Also for this orientation, the adoption of an unshaded clear glass produces high

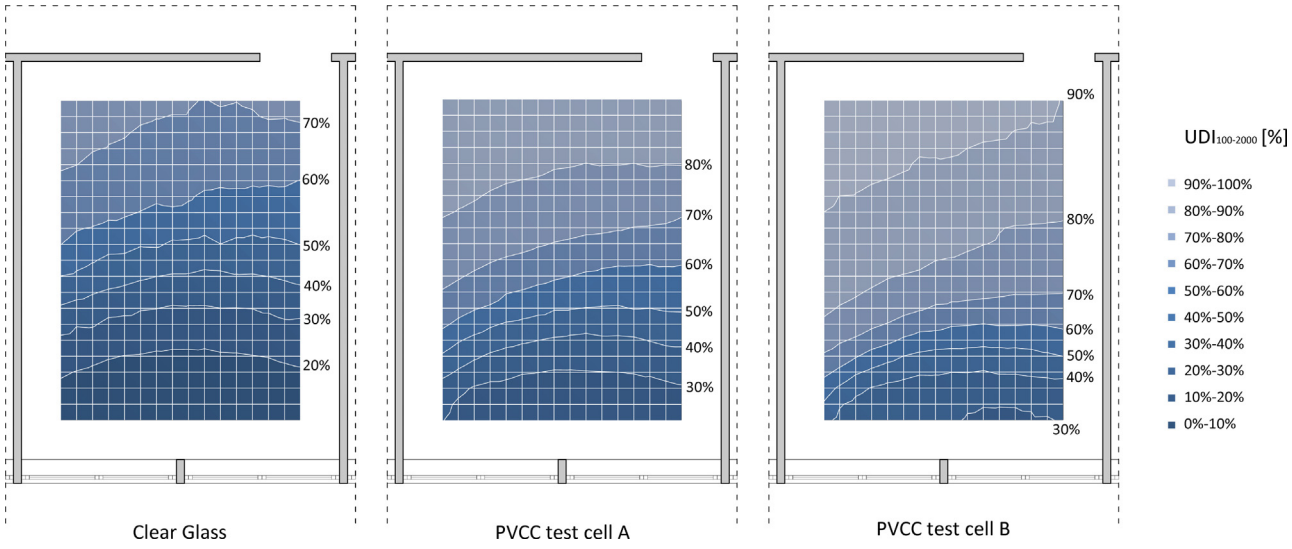

Fig. 5. Test room on east exposure: UDI during office hours (8.00–17.00).

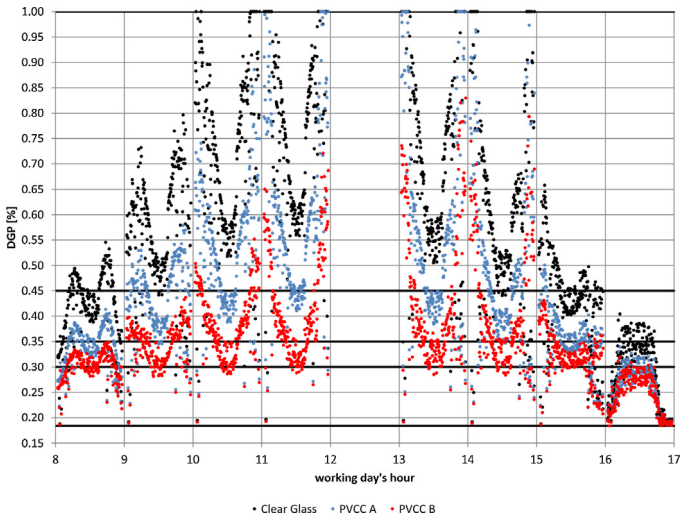

Fig. 6. Time-dependant DGP values for south exposure.

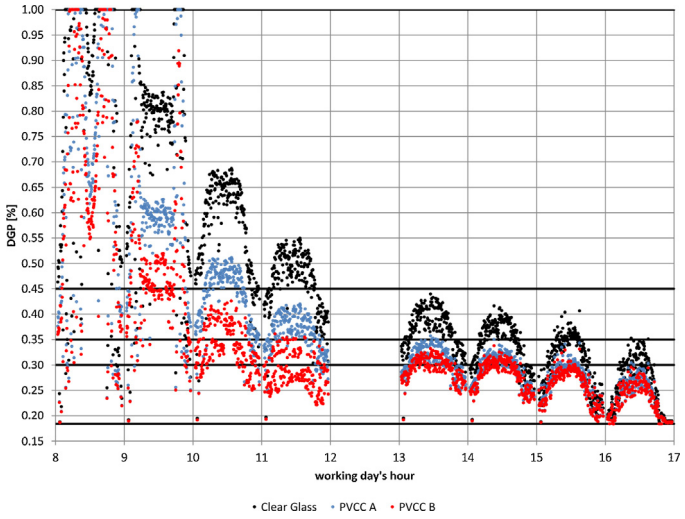

Fig. 7. Time-dependant DGP values for east exposure.

percentages of discomfort due to glare. In this case the effect is more evident in the first part of the morning, and a typical user would experience intolerable glare (UDI > 0.45) for more than 40% of the occupancy hours. The adoption of a photovoltachromic integrated window could determine a significant decrease of glare probability. As a matter of fact both the two devices which have been tested are able to reduce the DGP parameter. Integrating photovoltachromic devices A and B in a east-oriented window the percentage of hours in which an intolerable glare is experienced (DGP > 0.45) is reduced to respectively 26% and 17%. According to Fig. 7, the periods in which intolerable glare effects occur are all concentrated in the first hours of the morning (between 8 am and 10 am).

In conclusion, for the two orientations (south and east), in the following Table 5 the results of the visual comfort analyses carried out are summarized. The daylight distribution is represented as percentage of occurrence of excellent (75% < UDI < 100%), good (50% < UDI < 75%), average (25% < UDI < 50%) and poor (UDI < 25%) daylight distribution on the reference points during the working hours of the entire year. The glare perception is represented as the percentage of working hours in which an imperceptible (DGP < 0.3), perceptible (0.3 < DPG < 0.35), disturbing (0.35 < DGP < 0.45) or intolerable (DPG > 0.45) glare occurs for the reference view point.

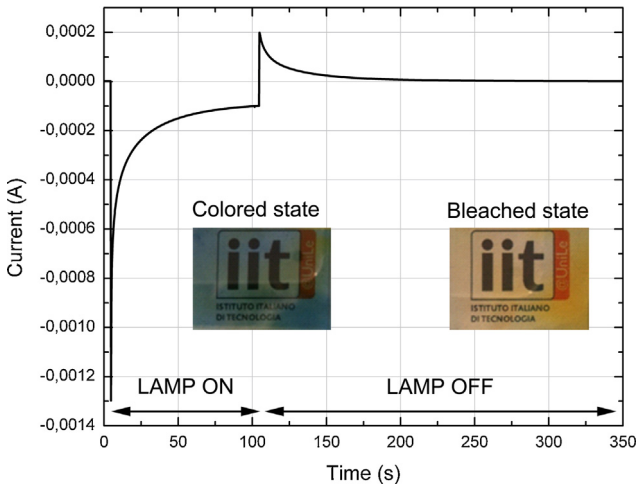

Fig. 8. Chronoamperometric curve of the photoelectrochromic circuit. It can be divided in three parts. At first, in dark, the device is short circuited. Then, the solar simulator lamp is switched off (100 mW/cm^2), then in the coloured state, at saturation, the lamp is switched off and bleaching takes place.

Both the devices are able to significantly improve indoor visual comfort condition, dynamically controlling solar radiation.

4.4. Electrical measurements

A detailed characterization of electrical performances was then carried out for devices containing a 300 nm thick tungsten oxide layer, whose electrochromic parameters were recognized as acceptable for further studies. Fig. 8 reports a chronoamperometric plot obtained by measuring the short circuit current in the photoelectrochromic circuit. Three main parts are clearly distinguishable. Before the lamp is switched on, the value of current is almost zero. When the light is switched on, a prompt increase in the value of current is noticed, followed by a sudden decrease to a roughly constant value, corresponding to the saturation of the colour-centres in tungsten oxide. In this condition, the electrochromic material is completely coloured. When the lamp is switched off, an inversion in the current flux is observed. The potential associated to the charge accumulated in the electrochromic material acts as a driving force for the bleaching process.

The real colour of the device is reported in the inset of Fig. 8. The colouration time is shorter than the one indicated on the diagram. The colouration of the device is almost completed after the time required to reduce the short circuit current by two thirds with respect to the initial value.

Fig. 9 shows the values of an important figure of merit in the characterization of photochromic devices: the photocolouration efficiency. In order to evaluate this parameter, we used the expression in Eq. (3) relating the efficiency with the optical density and the irradiance.

$$\eta = \frac{\Delta \mathrm{OD}}{G_t\, t} = \frac{1}{G_t\, t} \log\left(\frac{T_b}{T_c}\right) \tag{3}$$

where T_b and T_c represent the transmittance in the bleached and in the coloured state, respectively, G_t the total solar intensity for incidence normal to the device (W/cm^2), t the exposure time (min), assumed as the complete colouring time [38]. The latter value was taken from the chronoamperometric curve, corresponding to the attainment of the saturation current, in light. The values of colouration efficiency corresponding to wavelengths up to 500 nm are seriously affected by a blue shift in the transmission peak that can be observed between the bleached and the coloured state (comparison between Figs. 9 and 3b), which is commonly ascribed to

Table 5
Summary of daylight comfort analyses.

glass	exposure	daylight distribution				glare perception			
		excellent	good	average	poor	imperceptible	perceptible	disturbing	intolerable
Clear	South	0%	7%	41%	52%	9%	7%	18%	66%
	East	1%	45%	26%	27%	19%	15%	25%	41%
PVCC A	South	20%	23%	26%	32%	17%	13%	30%	40%
	East	36%	32%	25%	7%	37%	21%	16%	26%
PVCC B	South	53%	15%	12%	20%	26%	34%	28%	12%
	East	60%	20%	21%	0%	54%	20%	10%	16%

Table 6
Photovoltaic performances in different irradiation conditions.

Irradiance (W/m^2)	PCE (%)	Fill Factor	V_{OC} (V)	J_{SC} (mA/cm^2)	Power (mW/cm^2)
1000	4,17	0,50	0,75	11,01	4,22
700	4,67	0,58	0,75	7,90	2,00
400	4,32	0,68	0,74	3,42	1,43

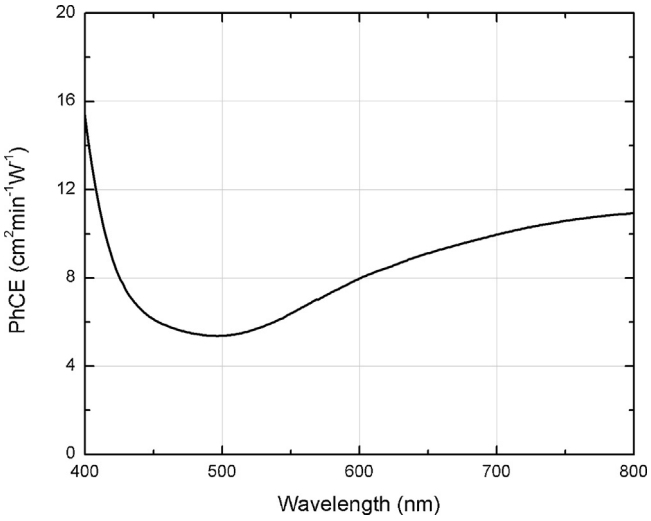

Fig. 9. Wavelength dependence of the colouration efficiency of the photoelectrochromic circuit. Higher results in the UV range (due to titanium dioxide).

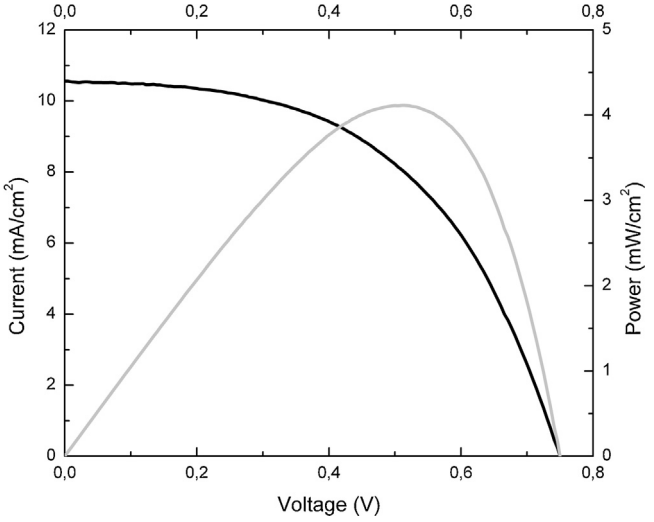

Fig. 10. *J–V* characteristics of the photovoltaic circuit.

the Burstein–Moss effect, consisting in a widening of the band-gap in tungsten oxide, due to electron and lithium insertion, during the colouration process [39]. The increase of colouration efficiency with larger wavelengths and its values throughout the visible range are comparable to those for WO_3 [38].

The characteristic *J-V* curve corresponding to the photovoltaic circuit of the photovoltachromic device is plotted in Fig. 10. A titanium dioxide photoelectrode having a thickness of 13 μm was used in this device. The power curve shows that the maximum power point corresponds to 0.47 V and a current of 8.60 mA/cm^2. The power provided by the photovoltaic circuit is not affected by the mechanism of colouration, which is self-supplied by its own circuit. In these operating conditions, the device can act both as a photovoltaic cell and as a photoelectrochromic cell.

Table 5 shows the effect of the variation of irradiance on the photovoltaic performances of the device. The fill factor increases linearly from 0.50 (at 1 sun) to 0.68 (at 0.4 sun). The increase of this parameter is related to the reduction of short circuit current due to lower irradiance available resulting in an attenuation of electron recombination. As already discussed in literature, Jsc increases linearly with radiant power whereas the fill factor increases when the radiant power is decreased (Table 6) [40].

At the end, the global energy production of a window equipped with test cell B has been calculated. Considering the typical days of each month, the highest benefits are obtained for the south exposure, for which the specific energy production varies in the range between 660 Wh/day and 876 Wh/day. For east exposures, as the test cell has a higher fluctuation of energy production (5.4–14.3 mWh/cm^2 day) depending on the season, transparent surfaces equipped with a PVCC glass B are able to produce an amount of energy that varies between 324 Wh/day and 858 Wh/day. Therefore during a typical year a 6 m^2 PVCC integrated window is able to produce respectively about 280 kWh and 223 kWh if exposed to south and to east.

The energy amounts are ideally calculated considering windows completely equipped with PVCC glasses. While energy losses due to direct solar energy reduction for overcast sky conditions have been taken into account, direct and indirect shadows produced by surrounding buildings are instead not considered in the previous calculations.

5. Conclusions

We implemented an effective method for multidisciplinary experimental research activities. Multifunctional photochromic and photovoltaic devices have been designed and characterized. The optical features were used as inputs for visual comfort assessment in test rooms. The results obtained were effectively employed as useful feedbacks for the experimental activity of devices. The

increase of the thickness of the layer of tungsten oxide is largely beneficial for building integration: a higher optical modulation is the major benefit. For this reason, the devices with 300 nm thick layers of tungsten oxide have been selected for further analyses and underwent a complete electrical characterization, reported in this paper. Devices showing a 4.67% photovoltaic conversion efficiency and an optical modulation of 50% at 700 nm are able to increase indoor natural light levels if integrated in window's glazings. Major benefits are achievable integrating photovoltacromics in south exposed windows, where the average UDI percentage increases more than 2.5 times (from 26.1% for the clear glass to 65.5% for the PVCC test cell B) and in parallel the percentage of hour of tolerable glare increase of about two times (from 34% for the clear glass to 60% for PVCC test cell B). Moreover the integration of these devices also on east exposed windows is largely beneficial. Furthermore the benefits, both in terms of indoor natural light levels optimization and of energy production, increase as the window/floor surface ratio increases.

Further research activity aiming at an enhancement of transparency in the bleached state is being carried out. The yellow shade of electrolytes – due to the redox iodine-iodide couple – can be a limit to building integration purposes. Investigations concerning other suitable redox couples to be used in the ion-mediator formulation are required for this kind of devices.

Moreover, visual comfort assessment simulations show that further experimental activity would be required to obtain devices showing higher transmittance modulation even in low irradiance conditions (i.e. less than 400 W/m^2).

References

[1] G.C. Granqvist, Handbook of Inorganic Electrochromic Materials, Elsevier Science B.V., Amsterdam (The Netherland), 2002.

[2] G.C. Granqvist, A. Azens, P. Heszler, L.B. Kish, L. Osterlund, Nanomaterials for benign indoor environment: Electrochromics for smart windows, sensors for air quality, and photo-catalysts for air cleaning, Solar Energy Materials & Solar Cells 91 (2007) 355–365, http://dx.doi.org/10.1016/j.solmat.2006.10.011.

[3] G.A. Niklasson, C.G. Granqvist, Electrochromics for smart windows: thin film of tungsten oxide and nickel oxide, and devices based on these, Journal of Materials Chemistry 17 (2006) 127–156, http://dx.doi.org/10.1039/b612174h.

[4] M. Boubekri, Daylighting, Architecture and Health. Building Design Strategies, Elsevier Architectural Press, Oxford (United Kingdom), 2008.

[5] A. Azens, C.G. Granqvist, Electrochromic smart windows: energy efficiency and device aspects, Journal of Solid State Electrochemistry 7 (2003) 64–68, http://dx.doi.org/10.1007/s10008-002-0313-4.

[6] M.N. Assimakopoulos, A. Tsangrassoulis, G. Guarracino, M. Santamouris, Integrated energetic approach for a controllable electrochromic device, Energy and Buildings 36 (2004) 415–422, http://dx.doi.org/10.1016/j.enbuild.2004.01.040.

[7] M.N. Assimakopoulos, A. Tsangrassoulis, M. Santamouris, G. Guarracino, Comparing the energy performance of an electrochromic window under various control strategies, Building and Environment 42 (2007) 2829–2834, http://dx.doi.org/10.1016/j.buildenv.2006.04.004.

[8] F. Gugliermetti, F. Bisegna, Visual and energy management of electrochromic windows in Mediterranean climate, Building and Environment 38 (2003) 479–492, http://dx.doi.org/10.1016/S0360-1323(02)00124-5.

[9] R. Baetens, B.P. Jelle, A. Gustavsen, Properties, requirements and possibilities of smart windows for daylight and solar energy control in buildings: a state-of-the-art, Solar Energy Materials & Solar Cells 94 (2010) 87–105, http://dx.doi.org/10.1016/j.solmat.2009.08.021.

[10] C. Bechinger, S. Ferrere, A. Zaban, J. Sprague, B.A. Gregg, Photoelectrochromic windows and displays, Nature 383 (1996) 608–610, http://dx.doi.org/10.1038/383608a0.

[11] A. Georg, A. Georg, U.O. Krasovec, Photoelectrochromic window with Pt catalyst, Thin Solid Films 502 (2006) 246–251, http://dx.doi.org/10.1016/j.tsf.2005.07.291.

[12] A. Hauch, A. Georg, S. Baumgartner, U. Opara Krasovec, B. Orel, New photoelectrochromic device, Electrochimica Acta 46 (2001) 2131–2136, http://dx.doi.org/10.1016/S0013-4686(01)00391-7.

[13] L. Hechavarria, N. Mendoza, M.E. Rincon, J. Campos, H. Hu, Photoelectrochromic performance of tungsten oxide based devices with PEG–titanium complex as solvent-free electrolytes, Solar Energy Materials & Solar Cells 100 (2011) 27–32, http://dx.doi.org/10.1016/j.solmat.2011.05.004.

[14] Y. Li, J. Hagen, D. Haarer, Novel photoelectrochromic cells containing a polyaniline layer and a dye-sensitized nanocrystalline TiO_2 photovoltaic cell, Synthetic materials 94 (3) (1998) 273–277, http://dx.doi.org/10.1016/S0379-6779(98)00013-7.

[15] J.J. Wu, M.D. Hsieh, W.P. Liao, W.T. Wu, J.S. Chen, Fast-switching photovoltachromic cells with tunable transmittance, ACS Nano 3 (8) (2009) 2297–2303, http://dx.doi.org/10.1021/nn900428s.

[16] Y. Liu, H. Shen, W. Chen, H. Wang, Y.J. Deng, D.H. Wang, Novel photoelectrochromic cells fabricated with wirelike photo-electrode, Chinese Science Bulletin 53 (20) (2008) 3173–3177, http://dx.doi.org/10.1007/s11434-008-0454-7.

[17] A. Cannavale, M. Manca, F. Malara, L. De Marco, R. Cingolani, G. Gigli, Highly efficient smart photovoltachromic devices with tailored electrolyte composition, Energy and Environmental Science 4 (2011) 2567–2574, http://dx.doi.org/10.1039/c1ee01231b.

[18] W.J. Lee, E. Ramasamy, D.Y. Lee, J.S. Song, Dye-sensitized solar cells: Scale up and current – voltage characterization, Solar Energy Materials & Solar Cells 91 (2007) 1676–1680, http://dx.doi.org/10.1016/j.solmat.2007.05.022.

[19] U. Knaak, T. Klein, The future envelope 1. A multidisciplinary approach, IOS Press BV, Amsterdam (The Netherlands), 2008.

[20] S. Yang, J. Zheng, M. Li, C. Xu, A novel photoelectrochromic device based on poly(3,4-(2,2-dimethylpropylenedioxy)thiophene) thin film and dye-sensitized solar cell, Solar Energy Materials & Solar Cells 97 (2012) 186–190, http://dx.doi.org/10.1016/j.solmat.2011.09.038.

[21] C. Wu, C.Y. Hsu, K. Huang, P. Nien, J. Lin, K. Ho, A photoelectrochromic device based on gel electrolyte with a fast switching rate, Solar Energy Materials & Solar Cells 99 (2012) 148–153, http://dx.doi.org/10.1016/j.solmat.2011.03.033.

[22] C. Hsu, K. Lee, J. Huang, K.R. Justin Thomas, J.T. Lin, K. Ho, A novel photoelectrochromic device with dual application based on poly(3,4-alkylenedioxythiophene) thin film and an organic dye, Journal of Power Sources 185 (2008) 1505–1508, http://dx.doi.org/10.1016/j.jpowsour.2008.09.031.

[23] L.M. Huang, C.P. Kung, C.W. Hu, C.Y. Peng, H.C. Liu, Tunable photovoltaic electrochromic device and module, Solar Energy Materials & Solar Cells 107 (2012) 390–395, http://dx.doi.org/10.1016/j.solmat.2012.07.021.

[24] S. Yoon, S. Tak, J. Kim, Y. Jun, K. Kang, J. Park, Application of transparent dye-sensitized solar cells to building integrated photovoltaic systems, Building and Environment 46 (2011) 1899–1904, http://dx.doi.org/10.1016/j.buildenv.2011.03.010.

[25] DAYSIM v. 3.1b (beta). www.daysim.com, 2012 (retrieved 12.04.12).

[26] C.F. Reinhart, O. Walkenhorst, Validation of dynamic RADIANCE-based daylight simulations for a test office with external blinds, Energy and Buildings 33 (2001) 683–697, http://dx.doi.org/10.1016/S0378-7788(01)00058-5.

[27] D. Bourgeois, C.F. Reinhart, G. Ward, Standard daylight coefficient model for dynamic daylighting simulations, Building Research & Information 36 (1) (2008) 68–82, http://dx.doi.org/10.1080/09613210701446325.

[28] G. Ward, Behavior of Materials in RADIANCE, 2004 http://www.radiance-online.org/learning/documentation/references.html (retrieved 06.05.13).

[29] Lawrence Berkeley Laboratory, The Radiance 4.1 Syntetic Imaging System, 2011 http://www.radiance-online.org/learning/documentation/references.html (retrieved 06.05.2013).

[30] A. Nabil, J. Mardaljevic, Useful daylight illuminance: a new paradigm for assessing daylight in buildings, Lighting Research and Technology 37 (1) (2005) 41–59, http://dx.doi.org/10.1191/1365782805li128oa.

[31] A. Nabil, J. Mardaljevic, Useful daylight illuminances: a replacement for daylight factors, Energy and Buildings 38 (2006) 905–913, http://dx.doi.org/10.1016/j.enbuild.2006.03.013.

[32] J. Wienold, J. Christoffersen, Evaluation methods and development of a new glare prediction model for daylight environments with the use of CCD cameras, Energy and Buildings 38 (2006) 743–757, http://dx.doi.org/10.1016/j.enbuild.2006.03.017;
J.A. Jakubiec, C.F. Reinhart, The 'adaptive zone' – a concept for assessing discomfort glare throughout daylit spaces, Lighting Research and Technology 44 (2) (2012) 149–170, http://dx.doi.org/10.1177/1477153511420097.

[33] M.R. Atif, J.A. Love, P. Littlefair, Daylight Monitoring Protocols & Procedures for Buildings, 1997 (NRC-CNRC report number NRCC-41369).

[34] U.S. Department of Energy, EnergyPlus Energy Simulation software – Weather Data, City of Bari Palese-Macchie, region Europe, country Italy, 2013 http://apps1.eere.energy.gov/buildings/energyplus/weatherdata_about.cfm (retrieved 07.01.13).

[35] J. Mardaljevic, Validation of a lighting simulation program under real sky conditions, Lighting Research and Technology 27 (1995) 181–188, http://dx.doi.org/10.1177/14771535950270040701.

[36] M.S. Burdis, J.R. Siddle, R.A. Batchelor, J. Gallego, Electrochromic device development for large-scale applications, Proceedings of SPIE – The International Society for Optical Engineering 2531 (1995) 11–18, http://dx.doi.org/10.1117/12.217331.

[37] P. Boyce, N. Eklund, S. Mangum, C. Saalfield, L. Tang, Minimum acceptable transmittance of glazing, Lighting Research and Technology 27 (3) (1995) 145–152, http://dx.doi.org/10.1177/14771535950270030201.

[38] G. Leftheriotis, G. Syrrokostas, P. Yianoulis, Development of photoelectrochromic devices for dynamic solar control in buildings, Solar Energy Materials & Solar Cells 94 (2010) 2304–2313, http://dx.doi.org/10.1016/j.solmat.2010.07.030.

[39] A. Subrahmanyam, A. Karuppasamy, Optical and electrochromic properties of oxygen sputtered tungsten oxide (WO_3) thin films, Solar Energy Materials & Solar Cells 91 (2007) 266–274, http://dx.doi.org/10.1016/j.solmat.2006.09.005.

[40] S.Y. Huang, G. Schlichthorl, A.J. Nozik, M. Gratzel, A.J. Frank, Charge Recombination in Dye-Sensitized Nanocrystalline TiO_2 Solar Cells, Journal of Physical Chemistry B 101 (14) (1997) 2576–2582.